High-resolution calorimetric study of phase transitions in chiral smectic-*C* liquid crystalline phases

Y. Sasaki,[1] K. V. Le,[2] S. Aya,[2] M. Isobe,[1] H. Yao,[3] C. C. Huang,[4] H. Takezoe,[2] and K. Ema[1,*]

[1]*Department of Physics, Tokyo Institute of Technology, O-okayama, Meguro, Tokyo 152-8551, Japan*

[2]*Department of Organic and Polymeric Materials, Tokyo Institute of Technology, O-okayama, Meguro, Tokyo 152-8552, Japan*

[3]*Department of Macromolecular Science and Engineering, Kyoto Institute of Technology, Matsugasaki, Sakyo-ku, Kyoto 606-8585, Japan*

[4]*School of Physics and Astronomy, University of Minnesota, Minneapolis, Minnesota 55455, USA*

(Received 2 October 2012; published 28 December 2012)

We carried out an improved characterization of phase transitions among chiral smectic-*C* subphases observed for various antiferroelectric liquid crystals by precise heat capacity measurements. It was found that the phase transitions are intrinsically first order exhibiting a remarkable heat anomaly which involves little pretransitional thermal fluctuation and a finite thermal hysteresis. On the other hand, we also noticed that the critical point of the smectic-C^*_α–smectic-C^* transition is induced by the destabilization of the smectic-C^*_α phase which couples with the fluctuation associated with the smectic-*A*–smectic-C^*_α phase transition.

DOI: 10.1103/PhysRevE.86.061704 PACS number(s): 64.70.M−, 65.40.Ba, 64.60.fh

I. INTRODUCTION

Since the discovery of antiferroelectricity in liquid crystals, study of antiferroelectric liquid crystals (AFLCs) exhibited by elongated chiral molecules remains of great interest from both scientific and technological points of view. A prominent feature in AFLCs is that the delicate balance of ferroelectric and antiferroelectric interplay shows variant chiral smectic-*C* (Sm-*C*) subphases characterized by the tilt-azimuthal angles from layer to layer [1]. Such a competing interaction, which prevents simultaneous minimization of the locally favored configuration, occurs in many physical systems, ranging from hard to soft materials [2]. Currently accepted sequence of the phases below the smectic-*A* (Sm-*A*) phase is the following; Sm-C^*_α–Sm-C^*–Sm-C^*_{FI2}–Sm-C^*_{FI1}–Sm-C^*_A. The Sm-C^*_α and normal Sm-C^* phases are characterized by an incommensurate helical structure, which can be distinguished by a short ($\sim$nm) and a long ($\sim\mu$m) pitch of the helix, respectively. The Sm-C^*_{FI2} and Sm-C^*_{FI1} phases, which appear between the Sm-C^* and antiferroelectric Sm-C^*_A phases, have four- and three-layer periodicity, respectively. Moreover, very recently, Wang *et al.* reported the observation of a six-layer smectic subphase by using some binary mixtures [3]. These rich polymorphisms make the study of AFLCs fascinating and challenging. Many experimental and theoretical works have been devoted to describing the phase sequence of AFLCs [1]. On the other hand, there are still many poorly understood phenomena that will be important information for the complete description of AFLCs. Particularly, whether the relevant molecular interaction is long-ranged or not is a long-standing question.

Among many experimental probes for LCs, thermodynamic investigation is a basic approach to characterize macroscopic properties of materials related to the energy fluctuation. However, past calorimetric studies on AFLCs could provide limited information because of experimental difficulties coming from smallness of heat anomalies and sluggish thermal response. Regarding this, we have recently shown that high-resolution differential scanning calorimetry (DSC) is a powerful tool for AFLCs [4,5], although experiments there were limited only to the Sm-C^*_α–Sm-C^* phase transition. In this work, we report a comprehensive heat capacity investigation on the phase transitions among chiral Sm-*C* subphases, which can be related to the behavior of the helical pitch.

High-resolution measurements revealed that phase transitions among chiral Sm-*C* subphases are intrinsically first order involving little thermal fluctuation as well as a significant thermal hysteresis. On the other hand, when the temperature width of the Sm-C^*_α phase is narrower, the first-order character of the Sm-C^*_α–Sm-C^* phase transition is weakened and moves towards a continuous behavior due to the thermal fluctuation associated with the Sm-*A*–Sm-C^*_α phase transition.

II. EXPERIMENT

The LC materials used in this work are [1,1'-biphenyl]-4-carboxylic acid, 4'-octyl-, 4-[[(1-methylheptyl)oxy]carbonyl]phenyl ester (MHPBC), [1,1'-biphenyl]-4-carboxylic acid, 4'-(octyloxy)-, 4-[[(1-methylheptyl)oxy]carbonyl]phenyl ester (MHPOBC), benzoic acid, 4-[[2-fluoro-4-(undecyloxy)benzoyl]oxy]-, 4-[[(1-methylheptyl)oxy]carbonyl]phenyl ester (11OHFBBB1M7, or denoted as 11OHF), benzoic acid, 4-[[4-(alkyloxy)benzoyl]thio]-, 4-[[(1-methylheptyl)oxy]carbonyl]phenyl ester (*n*OTBBB1M7, or denoted as C*n*), and (S)-(+)-1-methylheptyl 4-[2-(4-alkoxyphenyl) thiophene-5-carbonylthiooxy] benzoate (LN36). Their chemical structures are shown in Fig. 1. All the samples except for MHPOBC (Aldrich) [6] are laboratory synthesized. In each measurement, the amount of the sample used was 10–20 mg. A high-resolution DSC which has been built in our laboratory has been used for the measurement. This apparatus is based on the idea as described in Ref. [7]. Generally, in DSC, the heat absorption difference between a sample and a reference cell caused by a linear ramp of the temperature (dT/dt) is measured through thermoelectric sensors as an electric signal. As reported in Ref. [7], a very high-resolution measurement is realized by the use of semiconducting thermoelectric modules as the sensor. We have already shown that this method serves as an effective approach for the study of LC materials [8]. Here, we briefly describe our experimental setup used in this work.

*kema@phys.titech.ac.jp

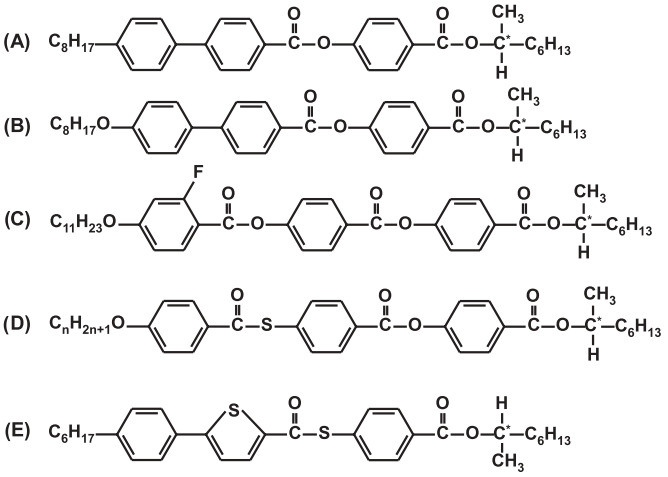

FIG. 1. Chemical structures of AFLCs used in this work: (A) MHPBC, (B) MHPOBC, (C) 11OHFBBB1M7 (11OHF), (D) *n*OTBBB1M7 (C*n*, $n = 11,12$), and (E) LN36.

Figure 2 shows the schematic illustration of the calorimeter. The thermal shields S1–S4 reduce the internal temperature fluctuation significantly, leading to a uniform increasing (decreasing) of the temperature of thermal bath B. The shield S4 is connected to a constant temperature water tank which suppresses the effect of the temperature fluctuation of the outside. The temperature control is conducted by a flexible heater H closely attached around S2. The sample and reference cells are placed on the semiconducting sensors T fixed on the thermal bath B. The cell structure is basically the same as used in Ref. [9]. A differential heat flux dQ/dt, which is associated with the heat capacity difference between the sample C_s and the reference C_r, is proportional to the corresponding temperature difference ΔT. The value of ΔT is also linked to the differential voltage $\Delta E = S\Delta T$ produced by the thermoelectric sensors with a thermoelectric power S. Then, the eventual relationship can be written with the following: $dQ/dt = \Delta T/R = \Delta E/(RS) = (C_s - C_r)dT/dt$, where R and dT/dt are the thermal resistance of the sensor and the temperature scan rate. When the temperature is held at a constant values (i.e., $dT/dt = 0$), nonzero value of dQ/dt corresponds to the resolution of the measurement. A typical behavior of baseline stability is shown in Fig. 3. In this case, $\Delta E \sim \pm 5$ nV and $RS \sim 0.25$ VW^{-1} eventually give rise

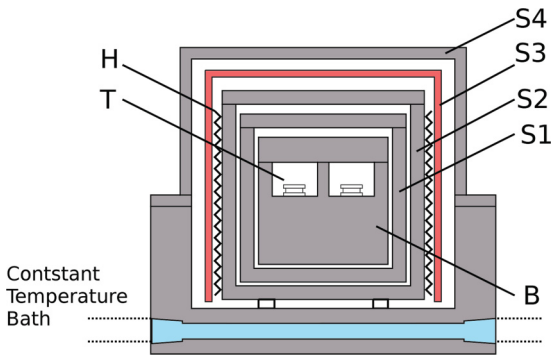

FIG. 2. (Color online) Schematic illustration of DSC. S1–S4 are thermal shields, B thermal bath, H heater, and T thermoelectric sensor.

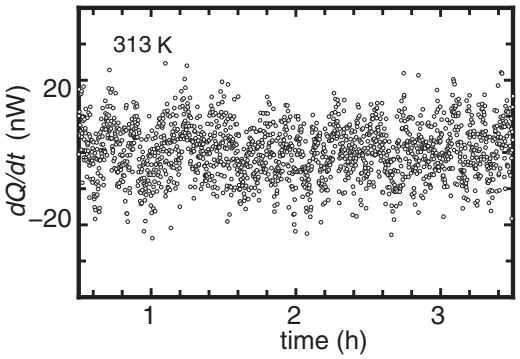

FIG. 3. Stability of the baseline as a function time. The temperature is fixed at 313 K.

to a resolution as small as ±20 nW. To approach the static conditions, $dT/dt = \pm 50$ mK/min is used. The obtained heat flow rate is converted into the specific heat capacity C_p data.

III. RESULTS

Figure 4 shows typical data for AFLC samples which show Sm-*A*–Sm-C^*_α–Sm-C^*–Sm-C^*_{FI2}–Sm-C^*_{FI1}–Sm-C^*_A phases. Here, C11.04 denotes the mixture of 96% C11–4% C12. The excess heat capacity ΔC_p is presented after subtracting the background heat capacity contribution from the net C_p behavior. It is seen that high-resolution calorimetric measurement succeeds in detecting all the thermal events and their characteristic shapes of anomalies depending on the transitions. The Sm-*A*–Sm-C^*_α transition involves a noticeable pretransitional wing in the heat capacity due to the thermal fluctuation. The non-Landau feature of the anomaly is clearly confirmed from the existence of the anomaly above the transition temperature. On the other hand, the heat anomaly at the Sm-C^*_α–Sm-C^* phase transition shows a significant material dependence. A rounded peak is found for C12, while the C11.04 and C11 exhibit much sharper peaks. Within our experimental resolution, the heat anomaly for Sm-*A*–Sm-C^*_α–Sm-C^* transitions showed a quite good agreement

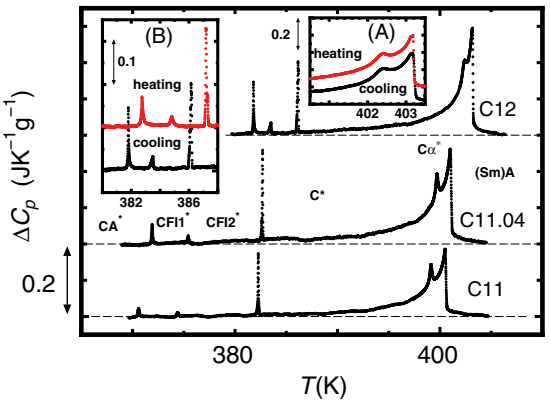

FIG. 4. (Color online) Excess heat capacity of AFLCs *n*OTBBB1M7(C*n*) near the Sm-*A*–Sm-C^*_α–Sm-C^*–Sm-C^*_{FI2}–Sm-C^*_{FI1}–Sm-C^*_A phases. Dashed line shows the background contribution. The insets (A), (B) show the enlarged views near the transition for C12. The heating data in the insets have been displaced vertically by 0.1.

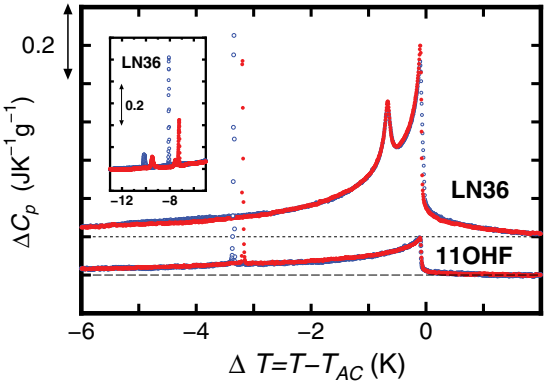

FIG. 5. (Color online) Heat anomalies near Sm-A–Sm-C^*_α–Sm-C^* phase transitions. Closed (red) and open (blue) circles show heating and cooling runs. T_{AC} shows the Sm-A–Sm-C^*_α transition temperature. The inset show the Sm-C^*–Sm-C^*_{FI1}–Sm-C^*_A phase transition for LN36.

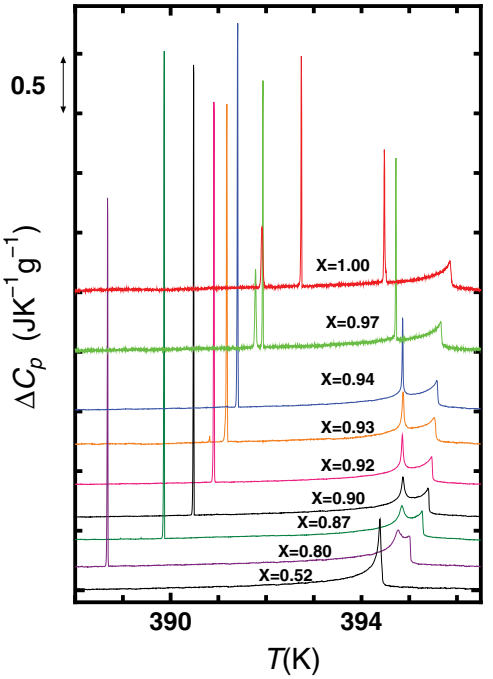

FIG. 6. (Color online) Heat capacity behavior of various MHPOBC enantiomeric mixtures upon cooling. Data points are plotted with lines connecting them. For $X = 0.52$, the Sm-C^*–Sm-C^*_A transition is observed ∼384.5 K (not shown). In cases of $X = 1.00$ and $X = 0.97$, the Sm-C^*_{FI1} phase exists between Sm-C^* and Sm-C^*_A phases [11]. It is to be noted that the $X = 1.00$ denotes 99% purity of (S)-enantiomer [6].

upon heating and cooling for C12 [see the inset (A)] and C11.04. A small thermal hysteresis of ∼20 mK was observed only for the Sm-C^*_α–Sm-C^* phase transitions of C11. This agrees qualitatively with an earlier report of resonant x-ray diffraction (RXRD) studies, where it has been argued that C11.04 is located near the critical point, and the behavior of C11 and C12 involves a small discontinuous and a continuous evolution in their pitch, respectively [10]. The observed Sm-C^*_α temperature width is 0.753, 1.363, and 1.372 K for C12, C11.04, and C11, which indicates that the temperature width of the Sm-C^*_α phase becomes smaller as the first-order character is weakened. These results suggest that the smearing of the peak occurs with decreasing the stability of the Sm-C^*_α phase. The other three peaks between Sm-C^*–Sm-C^*_A phases are quite sharp without pretransitional changes for all samples. They also show thermal hystereses of ∼1 K related to first-order nature of transitions [see the inset (B)]. Heat anomaly for the Sm-C^*_{FI2}–Sm-C^*_{FI1} is much smaller than those of the Sm-C^*–Sm-C^*_{FI2} and Sm-C^*_{FI1}–Sm-C^*_A phase transitions, indicating that the energy cost is relatively small.

Figure 5 presents the results of the other LC samples involving the Sm-C^*_α–Sm-C^* phase transition. LN36 shows the Sm-A–Sm-C^*_α–Sm-C^*–Sm-C^*_{FI1}–Sm-C^*_A phases and 11OHF the Sm-A–Sm-C^*_α–Sm-C^*. For LN36, heat anomalies for the Sm-A–Sm-C^*_α–Sm-C^* phase transitions show a good agreement upon cooling and heating. Delta-function-like sharp peaks are seen for the Sm-C^*–Sm-C^*_{FI1}–Sm-C^*_A phase transitions, while a sharp but cusplike anomaly is seen for the Sm-C^*_α–Sm-C^* transition. On the other hand, a distinctive first-order nature of the Sm-C^*_α–Sm-C^* phase transition is observed for 11OHF which contains a wide Sm-C^*_α phase and a small Sm-A–Sm-C^*_α heat anomaly.

To obtain further information, we also carried out systematic measurements on enantiomeric mixtures of MHPOBC and MHPBC. The detailed phase diagrams are found elsewhere [11,12]. Figure 6 presents the result of variant mixtures of (R)- and (S)-enantiomers of MHPOBC. Here, X denotes the weight fractions of the (S)-enantiomer. The overall trend is in agreement with the result in Ref. [5]. We note that the transition temperatures of the mixtures slightly increased compared to the previous work by carefully evaporating the solution [13]. We find that the transitions involving phases that exist at lower temperatures than the Sm-C^* phase always exhibit a quite sharp peak. On the other hand, the Sm-C^*_α–Sm-C^* heat anomaly changes its character depending on X, i.e., the anomaly rapidly loses the height and sharpness with decreasing X. It is seen that the temperature width of the Sm-C^*_α phase also decreases. In the present case, we expect that the critical point of the Sm-C^*_α–Sm-C^* transition is located $\sim X = 0.091$ by judging from the thermal hysteresis. To get a general view of this behavior near the Sm-C^*_α–Sm-C^* transition, we plotted in Fig. 7 the excess heat capacity accompanying the Sm-C^*_α–Sm-C^* phase transitions together with the corresponding transition enthalpy ΔH. We see that the thermal anomaly becomes broader as peak height decreases. The transition enthalpy reveals that first-order character shifts to the continuous behavior. It is remarkable that the magnitude of ΔH is independent of the concentration. The same tendency has been also found in MHPBC mixtures, although the data are not shown here. These observations strongly suggest that the width of the Sm-C^*_α phase plays an important role in determining the nature of the transition. We think it is probable that the stability of the Sm-C^*_α phase as well as the character of the Sm-C^*_α–Sm-C^* phase transition are affected by the chiral twisting power. We further took the behavior of the thermal hysteresis into consideration. Figure 8 shows the values of thermal hysteresis for the Sm-C^*–Sm-C^*_A and the Sm-C^*_α–Sm-C^* phase transitions. Here, δT is the temperature distance

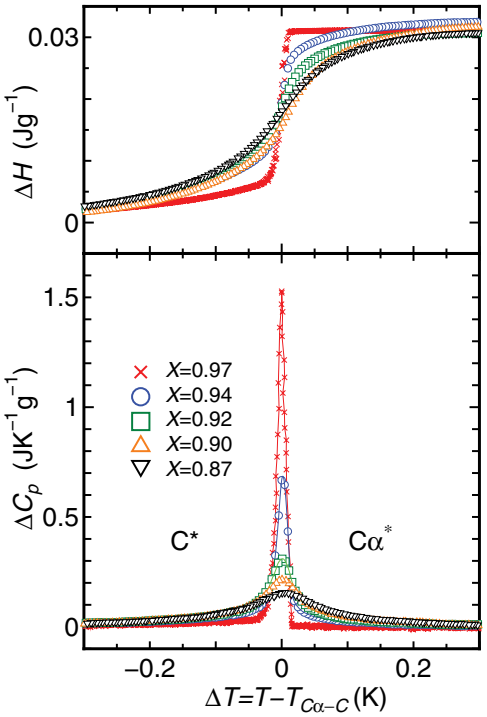

FIG. 7. (Color online) Excess heat capacity and transitional enthalpy of the Sm-C^*_α–Sm-C^* phase transition for several enantiomeric mixtures of MHPOBC upon cooling. $T_{C\alpha-C}$ shows the Sm-C^*_α–Sm-C^* phase transition temperature.

from the Sm-A–Sm-C^*_α phase transition. Our results show that the first-order character is more distinct moving away from the Sm-A phase for both cases of the Sm-C^*–Sm-C^*_A and the Sm-C^*_α–Sm-C^* phase transitions. This is all the more meaningful since the tendency is opposite when looking from the X dependence.

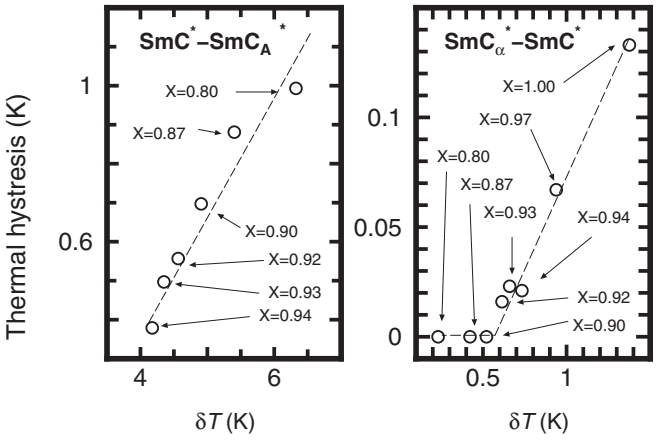

FIG. 8. Thermal hysteresis of the Sm-C^*–Sm-C^*_A and Sm-C^*_α–Sm-C^* phase transitions in (R)- and (S)-MHPOBC mixtures. The temperature scan rate is ±50 mK/min. In the figure, δT denotes the temperature distance from the Sm-A–Sm-C^*_α phase transition, determined using the transition temperatures on cooling. The result for $X = 0.52$ has not been included here, because the Sm-C^*_α phase is missing in that case. Dashed lines are guides to the eyes.

TABLE I. Values of the latent heat L obtained in cooling runs.

Substance	Transition	L (mJ/g)	L (J/mol)
C12	C^*–C^*_{FI2}	22.9	15.5
	C^*_{FI2}–C^*_{FI1}	4.9	3.3
	C^*_{FI1}–C^*_A	12.4	8.4
C11.04	C^*–C^*_{FI2}	19.8	13.1
	C^*_{FI2}–C^*_{FI1}	4.4	2.9
	C^*_{FI1}–C^*_A	8.9	5.9
C11	C^*–C^*_{FI2}	15.6	10.3
	C^*_{FI2}–C^*_{FI1}	2.5	1.6
	C^*_{FI1}–C^*_A	7.2	4.8
LN36	C^*–C^*_{FI1}	24.4	13.8
	C^*_{FI1}–C^*_A	10.9	6.1
MHPOBC($X = 1.0$)	C^*–C^*_{FI1}	35.7	19.9
	C^*_{FI1}–C^*_A	22.9	12.8
($X = 0.97$)	C^*–C^*_{FI1}	38.3	21.4
	C^*_{FI1}–C^*_A	23.3	13.0
($X = 0.94$)	C^*–C^*_A	60.5	33.8
($X = 0.93$)	C^*–C^*_A	61.9	34.6
($X = 0.92$)	C^*–C^*_A	61.7	34.4
($X = 0.90$)	C^*–C^*_A	56.7	31.6
($X = 0.87$)	C^*–C^*_A	55.4	30.9
($X = 0.80$)	C^*–C^*_A	49.6	27.7
($X = 0.52$)	C^*–C^*_A	36.7	20.5

Before concluding this section, most of the latent heat values obtained in the present work have been summarized in Table I. It is seen that the latent heat values are quite small for all the cases, being of the order of 10 J/mol, in agreement with the former results reported by several researchers (see, for instance, Refs. [14,15]).

IV. DISCUSSION

As shown above, our high-resolution DSC technique has proven to be quite effective in the study of phase transitions in AFLCs. It revealed the heat anomalies accompanying the phase transitions between Sm-A and Sm-C^* subphases. In particular, it was found that there exist two general trends as follows. (A) Except for the Sm-C^*_α–Sm-C^* transition, all transitions among chiral Sm-C phases are always first order, exhibiting a delta-function-like anomaly. (B) The heat capacity behavior associated with the Sm-C^*_α–Sm-C^* phase transition changes significantly depending on the liquid crystal system and the mixture ratio.

Starting with (A), this fact seems reasonable because, from symmetry considerations, the transition has to be first order for these cases. As discussed by Landau [16], for phase transitions of the second kind, the symmetry group of the lower symmetry phase has to be a subgroup of that of the higher phase, while this condition is not fulfilled in the transitions included in (A). In other words, for transitions discussed here, it is not possible to pass from one phase into another through a small local structure change which is caused by fluctuations. We also note that this explanation is compatible with observed quite small latent heat values, of the order of 10 J/mol, and pronounced thermal hysteresis for these transitions.

On the other hand, now considering (B), the situation is quite different in the Sm-C^*_α–Sm-C^* transition. It is known

that Sm-C^*_α and Sm-C^* phases have the same symmetry. Because of this, as observed, the phase diagram contains a first-order transition line which terminates at a critical point and supercritical evolution are found beyond that. It is worthwhile considering how the destabilization changes the nature of the Sm-C^*_α–Sm-C^* phase transition. In this context, we notice that the Sm-C^*_α–Sm-C^* phase transition is located on the pretransitional wing of the Sm-A–Sm-C^*_α anomaly. Thus it is reasonable to expect that the molecular fluctuation associated with the Sm-A–Sm-C^*_α phase transition couples with that of the Sm-C^*_α–Sm-C^* phase transition, leading to enhancement of the fluctuation. When the width of the Sm-C^*_α is narrower, the transition to the Sm-C^* occurs in a background with smaller smectic C order which favors the fluctuation associated with the Sm-C^*_α–Sm-C^* transition. This is a scenario similar in some sense to the case of the coupling of the smectic and nematic order. Indeed, the results revealed that the first-order character is more evident particularly when (i) the temperature width of the Sm-C^*_α phase expands and (ii) the transition enthalpy of the Sm-A–Sm-C^*_α phase transition decreases.

Finally, we mention the possibility that our present results would be helpful to understand the range of the interaction. Among many theoretical approaches for AFLCs, two theoretical models are known to successfully describe the phase sequence of AFLCs. One is the discrete phenomenological model [17] which is based on the short-range interactions and the other model is proposed by Hamaneh and Taylor [18] by taking the long-range interaction into account. It is pointed out that, when short- and long-range orders are competing, a locally favored state determined by short-range interactions prevents the long-range ordering [19]. This idea seems to be applicable to our situation and might suggest that the short-range interactions are effective to cause phase transitions in chiral Sm-C phases. However, it still remains unclear whether the long-range interactions should be considered. Various approaches should be required to obtain solid information.

In summary, precise heat capacity measurements on AFLCs have been carried out. It was revealed that phase transition among chiral Sm-C phases are intrinsically first order. Our results will be helpful to theoretical viewpoints to determine the range of the molecular interactions in chiral Sm-C phases.

[1] H. Takezoe, E. Gorecka, and M. Čepič, Rev. Mod. Phys. **82**, 897 (2010), and references therein.

[2] J. Sadoc, *Geometry in Condensed Matter Physics* (World Scientific, Singapore, 1990).

[3] S. Wang, L. D. Pan, R. Pindak, Z. Q. Liu, H. T. Nguyen, and C. C. Huang, Phys. Rev. Lett. **104**, 027801 (2010).

[4] Y. Sasaki, K. Aihara, K. Ema, H. Yao, and C. C. Huang, Ferroelectrics **395**, 60 (2010).

[5] Y. Sasaki, K. Aihara, M. Isobe, and K. Ema, Mol. Cryst. Liq. Cryst. **546**, 209 (2011).

[6] Commercial samples provide 99% purity for (S)-enantiomer and 98% purity for (R)-enantiomer.

[7] S. Wang, K. Tozaki, H. Hayashi, and H. Inaba, J. Therm. Anal. Cal. **79**, 605 (2005).

[8] Y. Sasaki, H. Nagayama, F. Araoka, H. Yao, H. Takezoe, and K. Ema, Phys. Rev. Lett. **107**, 237802 (2011).

[9] K. Ema and H. Yao, Thermochim. Acta **304-305**, 157 (1997).

[10] Z. Q. Liu, S. T. Wang, B. K. McCoy, A. Cady, R. Pindak, W. Caliebe, K. Takekoshi, K. Ema, H. T. Nguyen, and C. C. Huang, Phys. Rev. E **74**, 030702 (2006).

[11] E. Gorecka, D. Pociecha, M. Čepič, B. Žekš, and R. Dabrowski, Phys. Rev. E **65**, 061703 (2002).

[12] A. Cady, Z. Q. Liu, X. F. Han, S. T. Wang, M. Veum, N. Janarthanan, C. S. Hsu, D. A. Olson, and C. C. Huang, Phys. Rev. E **66**, 061704 (2002).

[13] The mixtures are obtained by evaporating a solution after ultrasonic agitation. The change in transition temperatures is attributed to the impurity effect due to the incomplete evaporation process. This leads to a slight difference in the expected location of the critical point compared to the earlier result in Ref. [5].

[14] K. Ema, H. Yao, I. Kawamura, T. Chan, and C. W. Garland, Phys. Rev. E **47**, 1203 (1993).

[15] S. Asahina, M. Sorai, A. Fukuda, H. Takezoe, Y. Suzuki, I. Kawamura, K. Furukawa, and K. Terashima, Liq. Cryst. **23**, 339 (1997).

[16] L. D. Landau and E. M. Lifshitz, *Statistical Physics, 3rd ed., Part 1* (Pergamon Press, New York, 1980), Chap. 145.

[17] K. Susman, B. Žekš, and M. Čepič, Phys. Rev. E **81**, 031701 (2010).

[18] M. B. Hamaneh and P. L. Taylor, Phys. Rev. Lett. **93**, 167801 (2004).

[19] H. Shintani and H. Tanaka, Nature Phys. **2**, 200 (2006).